AN INVESTIGATION INTO THE LOW CYCLE COMPRESSIVE FATIGUE FAILURE MECHANISM OF A COMPOSITE MATERIAL

Gerald Sedor

AN INVESTIGATION INTO THE LOW CYCLE COMPRESSIVE FATIGUE FAILURE MECHANISM OF A COMPOSITE MATERIAL

by

GERALD SEDOR

B.S., United States Naval Academy

(1957)

SUBMITTED IN PARTIAL FULFILLMENT

OF THE REQUIREMENTS FOR THE DEGREE OF

NAVAL ENGINEER

AND THE DEGREE OF

MASTER OF SCIENCE IN OCEAN ENGINEERING

AT THE

MASSACHUSETTS INSTITUTE OF TECHNOLOGY

June 1970

AN INVESTIGATION INTO THE LOW CYCLE COMPRESSIVE FATIGUE FAILURE MECHANISM OF A COMPOSITE MATERIAL

by

GERALD SEDOR

Submitted to the Department of Naval Architecture and Marine Engineering on May 21, 1970, in partial fulfillment of the requirements for the Master of Science Degree in Ocean Engineering and the Professional Degree, Naval Engineer.

ABSTRACT

The high strength-to-weight ratio of fiber reinforced plastics makes them highly attractive for deep submersible structural applications. Fatigue behavior may be a limiting factor in this application. The low cycle compressive fatigue behavior of a glass-epoxy orthogonal laminate, and the effects of sea water immersion on such a laminate, are investigated in this study.

Progressive damage during fatigue was invested by optical microscopy to develop a failure mechanism. Results of testing indicate that compressive fatigue strength decreases in a linear manner with an increase in fatigue cycles. No endurance limit is apparent in the range tested. The compressive fatigue strength was found to vary directly with fiber volume fraction and inversely with void content. The indicated strain increased linearly up to approximately 60 percent of fatigue life. Beyond this point a significant increase in strain rate was observed. Sea water immersion resulted in a decrease in compressive fatigue strength, probably by absorption into and degradation of existing voids.

The proposed failure mechanism is based on an initial debonding between individual fibers and matrix within plies where the fibers are oriented parallel to the load axis. Progressive debonding probably leads to local buckling of axial fibers, accompanied by the observed increase in strain rate. When cracks in the damaged axial plies are finally transmitted through the transverse plies, a slant type of shear fracture occurs.

Thesis Supervisor: JAMES W. MAR

Title: Professor of Aeronautics and Astronautics

ACKNOWLEDGMENTS

In the course of this study, the author received assistance and support from sources within four separate Departments at the Massachusetts Institute of Technology. An attempt will be made to acknowledge some of these sources.

In the Department of Aeronautics and Astronautics, Professor James W. Mar provided the initial guidance for this undertaking. His encouragement and advice as thesis supervisor were greatly appreciated. Assistance in the machining and testing of specimens was provided by Mr. Oscar Wallin.

The sound advice and suggestions of Dr. Lawrence A. Shepard, formerly with the Department of Metallurgy, were highly beneficial in the completion of this study. Instruction and advice in the use of photomicroscopy were provided by Mr. Guenther Arndt.

In the Department of Civil Engineering, advice and extensive reference materials were provided by Professor F. J. McGarry, while Mr. Arthur Rudolph provided assistance in specimen preparation. Mr. Richard Dauksys, a graduate student, proved to be a valuable source of information in the general area of composite materials.

The author's co-worker in the Department of Naval Architecture and Marine Engineering, LCDR Rodney K. Watterson, provided suggestions and a day-to-day sharing of problems which were invaluable throughout the entire investigation.

Finally, the author would like to thank his wife, Alma, for her patience and understanding during this study.

TABLE OF CONTENTS

LIST OF FIGURES

LIST OF TABLES

LIST OF SYMBOLS

SYMBOL	MEANING
c	Subscript for composite parameter
E	Young's Modulus
f	Subscript for fiber parameter
G	Shear Modulus
I_f	Moment of inertia of fiber column
L_f	Effective length of fiber
m	Subscript for matrix parameter
N	Number of fatigue cycles
P_{crit}	Critical buckling load
S	Fatigue stress
v	Void volume fraction
V_f	Fiber volume fraction
β_m	Spring constant for matrix
ϵ	Axial strain
σ_c	Compressive stress of composite
σ_{crit}	Critical stress for buckling
σ_d	Debonding stress
σ_{ULT}	Ultimate stress
μ	Poisson's ratio
γ	Volume percent
ρ	Specific gravity
ω	Weight percent

INTRODUCTION

Motivation and Application

The recent emphasis on the development of deep-diving hydrospace vehicles for scientific, commercial and military purposes has indicated the need for the development of structural materials with a high strength-to-weight ratio. Materials considered for this application include high strength metals, such as the alloys of steel, aluminum and titanium, as well as high strength nonmetallics such as glass, ceramics and composites of fiber-reinforced plastic.

Particular attention is being focused on glass reinforced plastic composites (GRP) by the United States Navy in the potential application to deep-diving submersible hulls. The primary interest in these materials lies in their very high strength-to weight ratios, which permit the construction of hull structures with acceptable low weight-to-displacement ratios and consequent high payload capabilities. For example, filament wound glass reinforced plastic laminates have been produced with compressive strengths of 170,000 psi and higher, providing strength-to-weight ratios in excess of 2×10^6 inches. In comparison, high strength steels (e.g., HY-140) have a ratio of 0.5×10^6 inches, while high strength titanium alloys (HY-120) have a ratio of 0.8×10^6 inches. (1)

In addition to the weight savings offered by the high specific compressive strength of GRP composite materials, these materials offer the capability of permitting tailor-made designs. Hence, the high strength capability may be built in only where required in the

particular application, thus effecting further savings in weight through the more efficient design of the material itself. (2)

The ultimate applicability of GRP composite materials, or similar materials, in the construction of deep submersible hulls will depend upon the reliability of performance of such materials under the operational requirements and environmental conditions encountered in such applications. Perhaps the most significant factor to be considered in this application is the high stress, low cycle fatigue associated with the necessity for repeated depth excursions of the submersible within the entire range of its depth capability. In this regard, Broutman and Krock state that "... the one type of behavior which appears more critical than the others and, indeed, may be a current limitation of the material, is its response to cyclic loads, or its fatigue life." (3)

While many other significant factors can and should be considered in evaluating the potential of GRP composite materials for hydrospace vehicle applications, this investigation will be limited primarily to the low cycle compressive fatigue characteristics of such materials, including the effects of sea water immersion on these characteristics. The techniques of photomicroscopy will be utilized to analyze prepared specimens at various stages of fatigue life in an attempt to determine the failure mechanism involved.

Theoretical Development and Background

Although the primary goal of this study is to develop a failure mechanism for an orthogonal composite material under a compressive fatigue loading, a limited theoretical development of the compressive strength of such a material will be presented.

A simplified analogy often used in the analytical treatment of compressive characteristics is that of the long slender fibers supported by the matrix viewed as slender columns supported by an elastic foundation. Timoshenko and Gere (4) have developed the relationship for critical buckling load of a column supported by an elastic foundation as:

$$P_{crit} = \frac{\pi^2 E_f I_f}{L_f^2} \qquad \text{(Equation 1)}$$

(See Table of Symbols for explanation of terms used in equations presented herein.)

From this relationship is developed the critical stress, σ_{crit}, corresponding to the critical buckling load:

$$\sigma_{crit} = \frac{1}{2}\sqrt{E_f \beta_m} \qquad \text{(Equation 2)}$$

where β_m is a spring constant assumed for the elastic foundation.

Two modes of local fiber buckling were described by Rosen (5). In the shear mode, the fibers are subject to buckling in an "in phase" interaction with the matrix. The critical composite stress for this mode is:

$$\sigma_{crit} = \frac{G_m}{1 - V_f} \qquad \text{(Equation 3)}$$

In the extension or transverse mode the fibers are subject to buckling in an "out of phase" interaction, with critical stress given by:

$$\sigma_{crit} = 2V_f \left[\frac{V_f E_m E_f}{3(1-V_f)}\right]^{1/2} \qquad \text{(Equation 4)}$$

For fiber volume fractions below approximately 0.17, the extensional mode is considered to be the controlling failure mode, while the shear mode is controlling for higher volume fractions. Discrepancies between these theoretical strengths and actual strengths of glass-epoxy composites were attributed by Rosen to the non-linear strain behavior of the matrix.

In testing boron-epoxy composites, Lager and June (6) were able to achieve excellent correlation between experimental results and theoretical predictions through the use of an "influence coefficient", or K_i, equal to 0.63. The use of an influence coefficient was justified on the basis that the idealized model assumes that all of the matrix is effective in resisting buckling, while the actual case results in out-of-phase effects.

A simple analysis of local buckling, in which a macroscopic model is employed, was presented by Foye. (7) In this analysis the composite shear modulus, G_c, is expressed in terms of the shear moduli of the constituent materials, with the resultant critical stress given by:

$$\sigma_c = \frac{G_f \; G_m}{V_f \; G_m + (1-V_f) \; G_f} \qquad \text{(Equation 5)}$$

In further development Foye was able to account for the significant effect of voids in reducing compressive strength. For a void content

of "v", the compressive strength is expressed by:

$$\sigma_c = \left\{ \frac{G_m}{(1-V_f) + V_f(G_m / G_f)} \right\} \left\{ \frac{1 - 2(\frac{v}{1-V_f})(\frac{v}{1-V_f})^2}{1 + (\frac{v}{1-V_f})} \right\}$$

(Equation 6)

The above equation clearly indicates the dependence of compressive strength on void content and shear stiffness, G_m , of the matrix.

Another type of failure, a debonding failure between fiber and matrix, can also occur when a composite material is subject to an axial compressive loading. Broutman and Krock (3) have expressed the debonding stress under an axial compressive load as:

$$\sigma_d = -\epsilon \left\{ \frac{(\mu_m - \mu_f) \; E_f \; E_m}{(1+\mu_m) \; E_f + (1 - \mu_f - 2\mu_f^2) \; E_m} \right\} \qquad \text{(Equation 7)}$$

The existence of microcracks at the glass-epoxy interface of a "Scotchply" type composite under axial compression was confirmed by Broutman (8) using an electron microscope. The cracks were determined to be less than 0.05 microns wide, and occurred at stresses representing less than 80% of ultimate compressive stress.

An analytical development of compressive fatigue behavior of composite materials has apparently yet to be developed. Indeed, as noted by Broutman and Krock (3), even a basic understanding of fatigue damage in glass-reinforced plastics is lacking.

Experimental observations of fatigue behavior in composite materials have generally concentrated on fatigue tests in which the mean stress has either been tensile or zero. In one study of com-

pressive fatigue behavior, Fried, et.al., (1) noted that water immersion of filament wound plastics resulted in a definite reduction in fatigue strength at stress levels below 80% of ultimate. Another study in which ultrasonic techniques were used to investigate damage under biaxial compressive fatigue loading has been described by Cole, et. al. (9) It is noted that almost all of the experimental work involving compressive fatigue of composite materials which is currently available in the literature has been accomplished under the sponsorship of the United States Navy with the ultimate application directed toward deep submersible structures.

PROCEDURE

Laminate Fabrication

The material used in the preparation of the cross-ply laminates was "Scotchply" Type 1002 prepreg tape obtained from the 3M Company. This is a high strength prepreg tape consisting of E-glass fibers in an epoxy matrix. Manufacturer's technical data on the characteristics of this material may be found in Appendix A.

The material was obtained in the form of unidirectional rolls of 12-inch width. To prepare the laminate, the Scotchply roll was cut into sections of 12-inch length. The paper liners were removed from each 12-inch square, and the plies laid alternately at zero degrees and ninety degrees to form the cross-ply laminate. Approximately thirty plies were used to obtain a single laminate with a cured thickness of about one-quarter inch. In an attempt to reduce entrapped air within the laminates, and thus reduce void content, all laminates subsequent to Laminate 6 were assembled using a "rolling pin" technique, applying a slight pressure as each ply was added to the laminate.

The 12-inch square laminate was then completely wrapped in a special release paper (3M Company, Type FC-400) and then sealed in a mylar covering. Due to an insufficient supply of the special release paper, Laminate 11 was assembled using a spray-type mold release agent (Fre Kote 33, Fre Kote Inc.) in lieu of the release paper.

The laminate sealed in the mylar covering was then placed between two flat aluminum plates, each approximately 12-inches square and one-quarter inch thick. The assembled "sandwich" was then placed

between the platens of a hydraulic compression press maintained at 350° F and allowed to warm up for a 5 minute period. The platens were then closed to maintain a slight pressure, which was gradually increased to 30 psi in a 5 minute period. This pressure was maintained for 10 minutes. The "sandwich" assembly was then removed from the hydraulic press and allowed to cool at atmospheric pressure and temperature.

A post cure cycle of 16 hours at 280° F is recommended by the manufacturer. As described in the manufacturer's Technical Data (10) elimination of this post cure cycle should result in a finished laminate with mechanical properties approximately 85% of specified design values. Based on this information, as well as the nature of the investigation, it was decided to eliminate the post cure cycle.

Specimen Shape and Preparation

Since the ASTM Test Methods do not specify a standard specimen shape for compressive fatigue of fiber reinforced plastics, a review of available literature was conducted to assist in the selection of an appropriate shape. After experimenting with various sizes and shapes of specimens found in the literature, the specimen geometry shown in Figure 1 was selected. It is based on the fatigue specimens used by Boller in his fatigue studies (11) (12), modified in length and width to eliminate the end sections which are fitted into a clamp for tensile testing. Since this study was to be limited to compressive stresses, it was determined that clamping of the ends would not be required and a shorter specimen would more closely

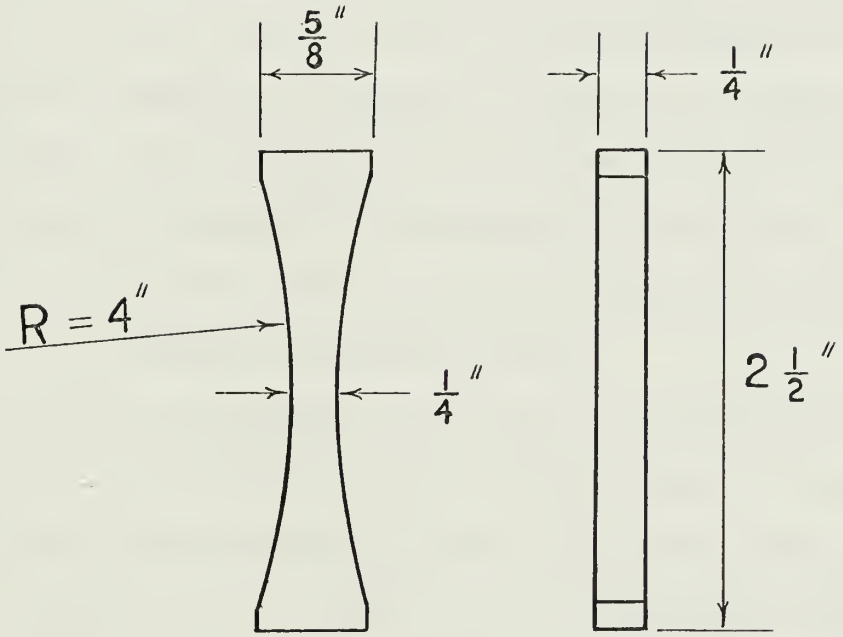

Figure 1. Fatigue Specimen Geometry

approach the relative dimensions of the compressive specimen described in the ASTM Test Methods. (13)

The fatigue specimens used by Broutman and Sahu in their study (14), although similar to that used by Boller, provided for a gage section of constant width and two inches in length. This shape was rejected in favor of Boller's shape, based on the desire to conduct a microscopic analysis of specimens which had been fatigued to less than failure. The varying cross-section area of the selected shape was considered advantageous in locating more precisely the section most likely to suffer fatigue damage, and consequently of more interest in subsequent microscopic analyses.

To prepare the specimens in the desired shape, the 12-inch square laminate was first cut into rectangular shapes of approximately the desired dimensions by means of a circular diamond abrasive wheel. Care was taken to ensure that all cuts were made along the axis of either the zero degree plies or the ninety degree plies. A Tensil-Kut machine was then used to obtain the required rectangular dimensions. Particular care was taken to ensure that the edges to be loaded were smooth, flat, and parallel, as specified in the ASTM Test Methods for compressive testing. (13) The specimens were then machined to provide for the desired radius of curvature, with a one-quarter inch width at the minimum section.

Fatigue Testing

The testing machine used for compressive and fatigue testing was a Baldwin SR-4 Compression and Tension Testing Machine, with test load readout and automatic cycling capability, in which upper and lower load limits can be set. To eliminate the effects of any misalignment of the specimen in the machine, a ball-joint surface was installed in the upper cross-head. This consisted of a machined steel hemisphere mounted in a hemispherical cavity and capable of rotation to any plane direction.

To prevent buckling of the specimens under compression, a support jig was used. The support jig design was based on that shown in Figure 4 of ASTM Test Method D 695 - 68T, modified to suit the dimensions of the specimen.

For indication of specimen strain under load, a dial gage extensometer was attached to the upper cross-head. The use of strain gages was precluded by the installation of the support jig. However, since strain data was not essential to the primary purpose of the study, but only served as a gross indicator of proximity to fatigue failure, the dial gage installation was considered entirely adequate. The test apparatus and support jig are shown in Figure 2.

The basic objective in testing was to first establish the ultimate compressive strength and compressive fatigue S-N Curve (Compressive Stress versus Number of cycles to failure) for each laminate. Progressive damage within the material could then be investigated by cycling the specimens at some arbitrary percent of ultimate compressive strength, stopping the cycling at various stages of fatigue life

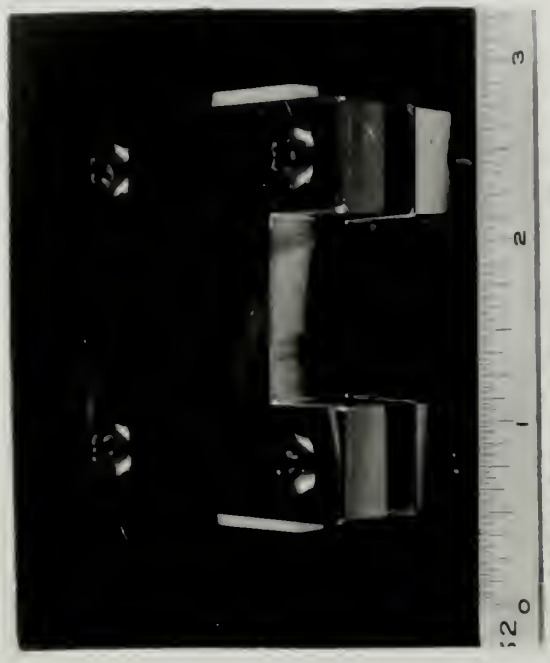

Figure 2a

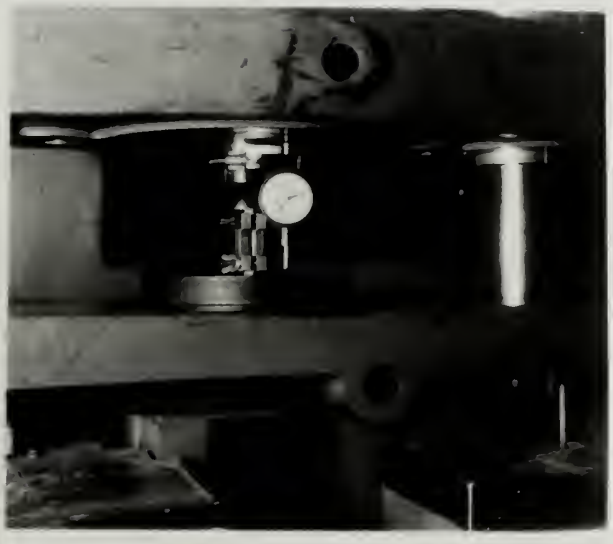

Figure 2b

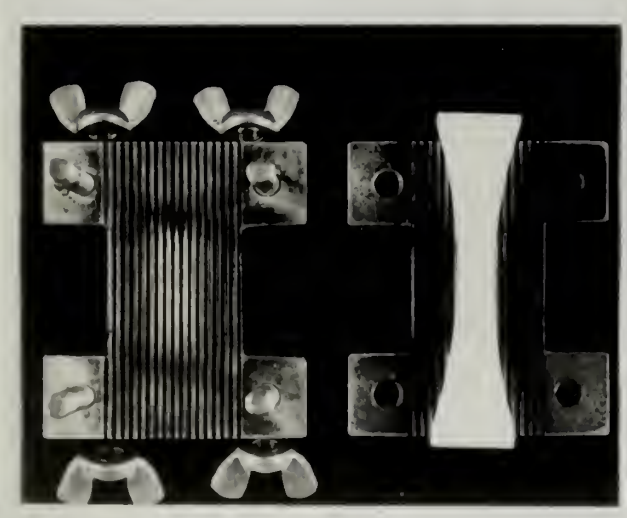

Figure 2c

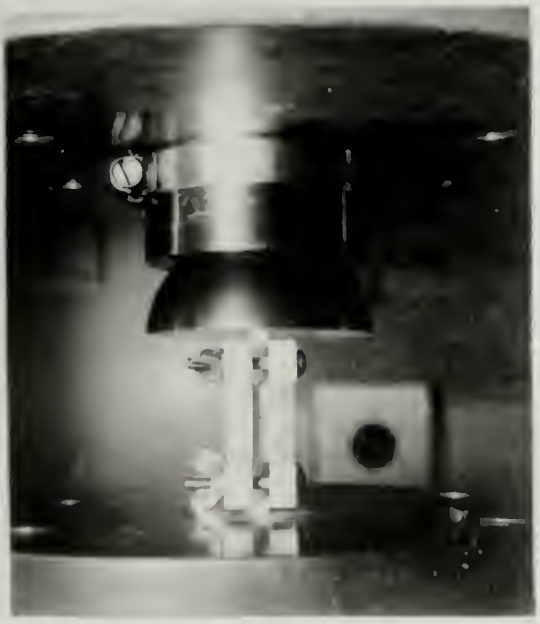

Figure 2d

Restraint Device and Testing Rig

before failure. The stress level selected was 75 $\pm$ 5% of ultimate compressive stress. The number of cycles to which a particular specimen was cycled was chosen arbitrarily, with strain data providing some indication as to the proximity to failure.

The calculated load for the particular stress desired could be pre-set into the machine to within approximately 15% of the desired value. The maximum load setting was generally refined within the second or third cycle to more closely approach the desired level. The lower limit for all fatigue cycling was set at approximately 1 to 3 % of ultimate compressive stress. The cycling rate for all tests was set at approximately 6 cycles per minute. This cycling rate was also used for the half-cycle tests for ultimate compressive strength.

After cycling the specimens to failure, or to the desired level before failure, the machine was stopped and the specimens removed and sectioned for microscopic analysis.

Environmental Testing

To investigate the effects of sea water immersion on the laminate, specimens from Laminate 11 were fully prepared, weighed, and completely immersed in a glass jar containing sea water obtained from the Nahant Beach area. To achieve the most severe effects of immersion, specimens were immersed with all cut edges exposed to the sea water. The immersed specimens were maintained at atmospheric pressure and room temperature throughout the entire immersion period of 21 days. A longer immersion period would probably

have been more effective in emphasizing the effects of immersion, but time constraints on this study limited the immersion period to 21 days.

Upon completion of the immersion period, the specimens were immediately weighed and fatigue tested, using the same testing procedures used for the other specimens. Selected specimens were then sectioned for microscopic analysis.

Measurement of Void Content

Void content of each laminate was determined by resin burnout and wet weighing techniques. The characterization formulas described by Cole, et. al., (9) were used and are listed below.

$$\text{Composite Specific Gravity } (\rho_c) = \frac{\text{Weight in Air}}{\text{Weight in Air} - \text{Weight in Water}}$$

$$\text{Resin Volume \%} = \left[\frac{\text{Resin Weight \%}}{\text{Resin Specific Gravity}}\right]\left[\text{Composite Specific Gravity}\right]$$

$$\text{or,} \quad \gamma_R = \frac{\omega_R \rho_c}{\rho_R}$$

$$\text{Similarly, Glass Volume \%} = \gamma_G = \frac{\omega_G \rho_c}{\rho_c}$$

$$\text{Void Volume \%} = 100 - (\text{Resin Volume \%} + \text{Glass Volume \%})$$

$$\text{or,} \quad \gamma_V = 100 - \gamma_R - \gamma_G$$

$$\text{Then,} \quad \gamma_V = 100 - \rho_c \left[\frac{\omega_R}{\rho_R} + \frac{\omega_G}{\rho_G}\right]$$

Glass fiber weight was determined by burning off the resin at 630° C and weighing the residue. In order to achieve accurate

results, two parameters must be known accurately, the specific gravity of the resin and the specific gravity of the glass fibers. The typical specific gravity of an E-glass fiber is given by Broutman and Krock (3) as 2.54 $\pm$ .03. However, as shown by Otto (15) , the density of E-glass is increased by heat treating, due to the compaction of glass at elevated temperatures. This density change remains when the glass is cooled to room temperature. The resin burnout technique used to determine void content, then, changes one of the "constants" used in subsequent calculations. Using Otto's results, a value of 2.59 was selected for the specific gravity of the glass fibers.

The other parameter of resin specific gravity is also subject to some question. The specific gravity of Type 1002 resin is listed in one 3M Company Memorandum as 1.16, with the qualifying remarks that the properties of the resin casting for which the data is given would not necessarily be totally indicative of the properties of the resin portion of a glass reinforced laminate molded under pressure with the resin in thin layers around and between fibers. (16) Other technical data of the 3M Company, as extracted in Appendix A, indicates that a composite specific gravity of 1.84 is achieved with a resin content of 36% by weight. Using this information with the assumed fiber specific gravity of 2.59, the resin specific gravity was calculated to be 1.26. This latter figure is used in all void content calculations.

Since the assumed values of resin and fiber specific gravity were somewhat questionable, it was decided to conduct a separate void content determination using an alternative method. The methods

of quantitative microscopy employed in this regard. According to DeHoff and Rhines (17), the systematic point count is the superior method for this application. This conclusion is further confirmed by the evaluation conducted by Hilliard and Cahn (18).

To conduct the point count, a two inch square grid was constructed on a clear plastic sheet. Ten grid lines were drawn in each direction, resulting in 100 grid corners. The size of the grid and the number of corners were based on optimum considerations outlined by Hilliard and Cahn, with the assumption that void content was approximately 3%.

To calculate void content, the grid was placed over randomly selected sections of the photomicrographs of the reference specimens. The total fraction of grid corners falling on void spaces then provided an unbiased estimate of the void volume fraction. The results of this method are compared with those of the resin burnout method in the Summary of Results.

Microscopic Analysis

The central portion of the fatigued specimens and reference specimens was sectioned for microscopic study by use of the diamond abrasive wheel. For each specimen to be analyzed, at least two sections were usually cut, one section parallel to the direction of applied load and one section perpendicular to the direction of the applied load. Figure 4 shows the relative orientation of the sections.

The sections were mounted in Quickmount and then rough polished by hand, using varying grades of silicon carbide polishing paper. A smoother polish was then obtained on a polishing wheel, using diamond pastes of 3 micron and 1/4 micron size and rinsed with kerosene. Final polishing was accomplished using the vibratory Syntron polisher with a 0.3 micron aluminum oxide polishing powder in distilled water.

Microscopic examinations of the posished specimens were accomplished using a Reichert Optical Metallograph. A Polaroid camera attachment was used to photograph each section. To provide the desired contrast and detail, a Nomarski interferometer with appropriate filters was installed. A magnification of approximately 120X was determined to be suitable. Actual magnification was determined by comparison of the photographs with a gage scribed at 0.01 mm intervals

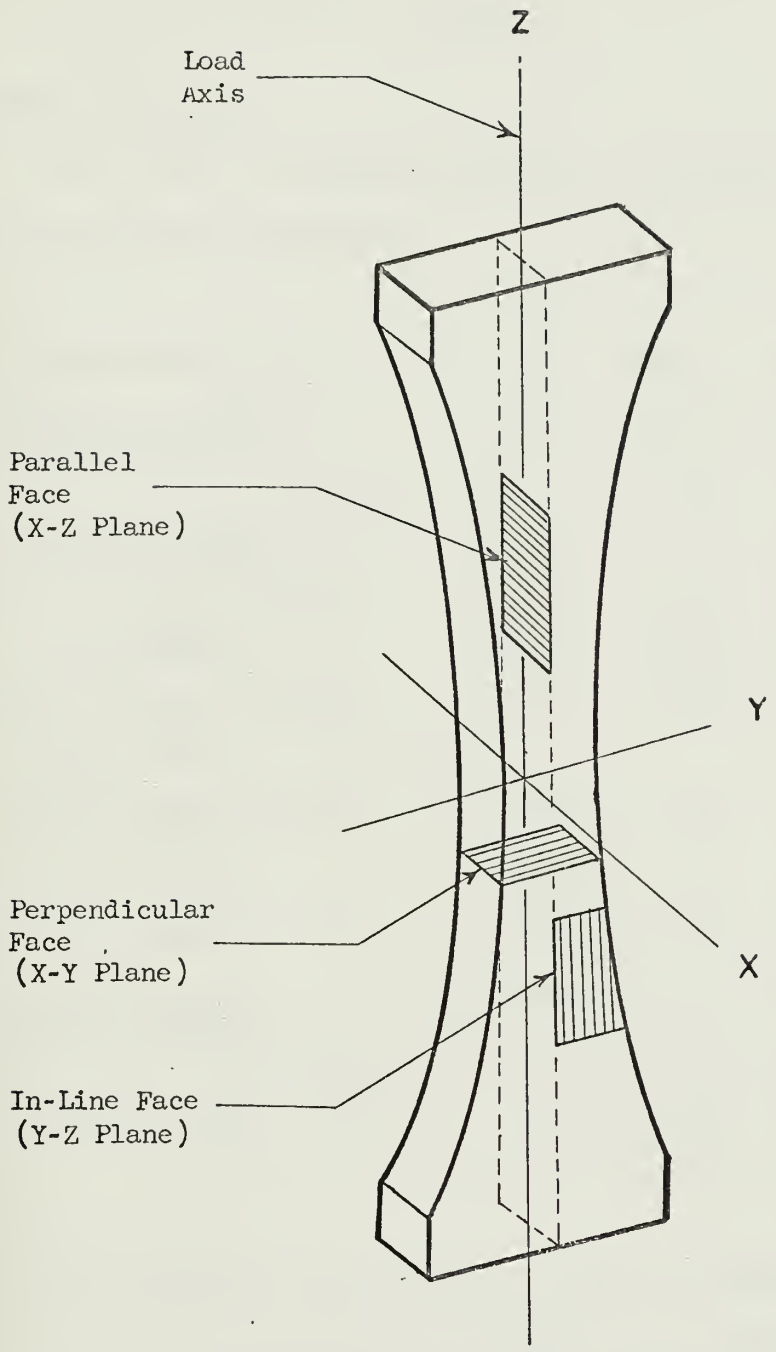

Figure 4. Orientation of Sections for Microscopic Analysis

RESULTS

Summary of Results

The results of laminate fabrication and testing are summarized in the following tabulation.

Laminate Number	6	10	11	11(SW)*
Ultimate Compressive Strength (psi)	70,300	83,200	89,000	77,800
Range of Cyclic Testing (Maximum cycles)	600	167	120	114
Void Content, Average (% by volume)	6.55 (8.50)	2.40 (5.33)	2.25 (4.67)	2.60 (6.15) #
Resin Content, Average (% by weight)	33.5	24.5	22.5	22.8
Fiber Content, Average (% by weight)	66.5	75.5	77.5	77.2
Fiber Volume Fraction (% by volume)	45.9	58.6	61.1	60.7
Specific Gravity, Cured, Average	1.79	2.01	2.05	2.03
Strength-to Weight Ratio (inches X 10^6)	1.09	1.15	1.20	1.06

* Indicates data for Laminate 11 after sea water immersion

\# Void content figures in parentheses calculated by quantitative microscopy, using two dimensional systematic point count method. Other figures indicate results of resin burnout method.

Macroscopic Failure

On a macroscopic level, failures under compressive or compressive fatigue loading were generally indicative of a shear mode of failure when the specimens were restrained from buckling by using the support jig shown in Figure 2. The shear line generally occurred near, but not precisely centered about, the section of minimum area. Three basic variations in shear failure were observed:

(1) A slant fracture type of shear rupture along a single fracture plane inclined approximately 45 degrees to the load axis.

(2) A double slant fracture, or "single V", with either side of the V inclined at approximately 45 - 60 degrees to the load axis, and extending throughout the thickness of the specimen.

(3) A multiple slant fracture, or "double V", in which a second V is added to the single V fracture, usually extending through only part of the thickness.

Typical examples of the above variations in shear failure can be seen in Figure 3. A fourth type of failure, not shown, occurred when the support jig was not used. In this case, failure occurred by delamination and buckling of individual plies, usually starting at the outer surface plies and progressing inward toward the center of the specimen.

Failures were generally accompanied by a very sharp cracking noise with a simultaneous rapid decrease in load indication. In some of the fatigue tests, a very slight cracking noise was heard at a varying number of cycles prior to ultimate failure. This noise was generally not accompanied by a significant decrease in

load indication. However, the indicated strain generally showed a rapid increase during subsequent cycling up to the point of failure. The actual failure point was defined as that point when a rapid decrease in applied load indication was observed, and in all cases was accompanied by a characteristic cracking noise.

Another macroscopic phenomenon observed was the formation of transverse lines and very fine cracks in an outer surface ply when this ply was assembled with its fibers oriented at 90 degrees to the load axis. The observed lines were parallel to each other and normal to the load axis, and extended throughout the entire width of the surface ply. In some failed specimens, the shear fracture appeared to originate from such a crack, but no consistency was observed in this regard.

The transverse lines or cracks were observed in fatigued specimens, in which cycling was stopped prior to failure, as well as in failed specimens. These lines were particularly noticeable in Laminate 11, in which an even number of alternating plies (32 plies) were used in fabrication. Hence, one surface ply was oriented with its fibers parallel to the load axis, while the fibers in the other surface ply were oriented normal to the load axis.

In an attempt to determine the effect of this transverse cracking on the fatigue strength of the laminate, the particular surface ply subject to this cracking was removed from several specimens by light sanding. Although this eliminated the transverse lines in the outer ply during subsequent tests, no significant effect on laminate strength was noted.

Microscopic Failure

Microscopic analyses were conducted on sections of selected specimens at various stages of fatigue life in order to investigate progressive damage of the material under compressive fatigue loading. Figures 5 through 19 are photomicrographs of some of the specimens which were examined, of which Figures 17, 18 and 19 represent specimens subject to sea water immersion prior to testing.

An analysis of the photomicrographs and their application to the development of a compressive fatigue failure mechanism are included in the Discussion of Results.

Compressive Fatigue Tests

The results of fatigue testing of a material are generally presented in the form of a curve showing fatigue stress versus the number of cycles to failure at that stress. Such "S - N Curves" are plotted for Laminates 6, 10, and 11 in Figures 20, 21, and 22 respectively. By normalizing fatigue stress to a percentage of ultimate compressive stress, the results for all three laminates are combined in Figure 23. The results of fatigue testing Laminate 11 prior to and subsequent to sea water immersion are compared in the S-N Curve of Figure 24. A summary of data for fatigue tests can be found in the tables of Appendix B.

In reviewing the S-N curves, it should be noted that the ultimate compressive stress for each laminate was arbitrarily defined as the highest compressive stress sustained by any of the specimens of that laminate prior to failure. In addition, it should be noted that

all S-N curves were arbitrarily started at one cycle. Those failures indicated on the curves as occurring on the first cycle could more accurately be shown as occurring at the first half-cycle, when the peak compressive load is applied.

An examination of the S-N curves indicates that, within the range tested, fatigue strength decreases in approximately a linear manner with an increase in fatigue cycles, on the semi-logarithmic scale used. No apparent endurance limit is observed in this range. Laminates 10 and 11 exhibited comparable fatigue strengths, with Laminate 11 having a slightly higher ultimate compressive strength. Laminate 6, while exhibiting an S-N slope similar to the other laminates, had a fatigue strength approximately 20% less than Laminates 10 and 11 throughout the range tested.

The immersion of specimens in sea water for the 21-day immersion period resulted in an average water absorption of 0.226% by weight, as summarized in Table 5 of Appendix B. Compressive fatigue strength for the immersed specimens showed a decrease of approximately 6 to 10 % throughout the range tested, as shown in Figure 24.

The strain history of selected specimens, shown in Figure 25, indicates that the strain increases in an almost linear manner up to approximately 60% of the fatigue life of the material. Beyond this point, there is a marked increase in the rate of strain increase with increased cycling. The strain data is listed in Table 4 of Appendix B.

Figure 3a

Figure 3b

Figure 3c

Typical Failures

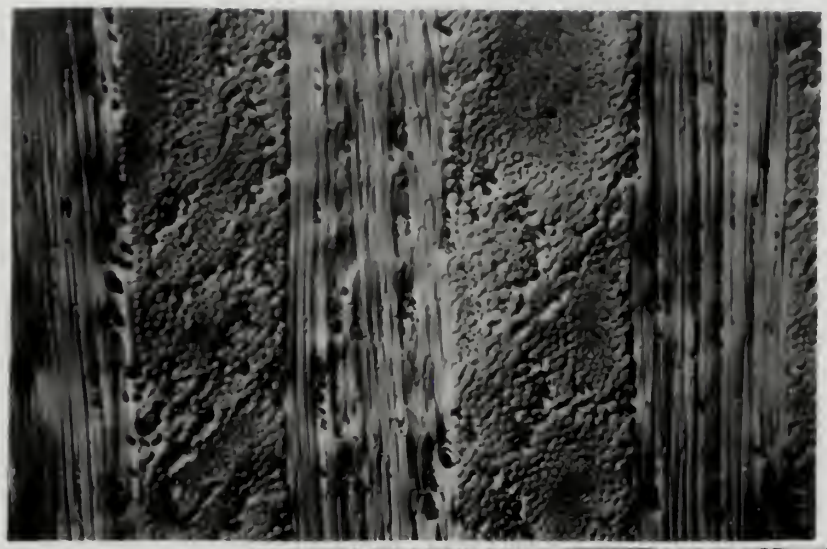

Figure 5

Laminate #11

Reference

120X

Parallel Face

Figure 6

#11 BE

69,400 psi

20 Cycles

No Failure

120X

Parallel Face

Load Direction

is Vertical

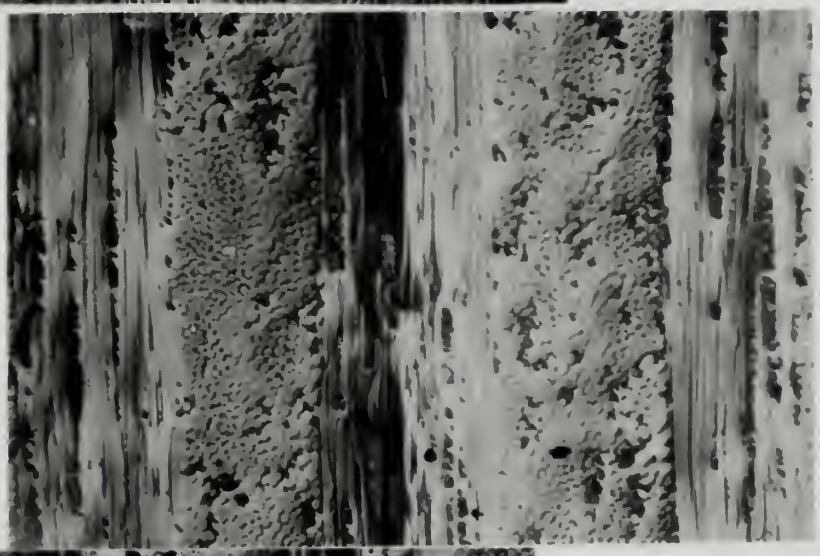

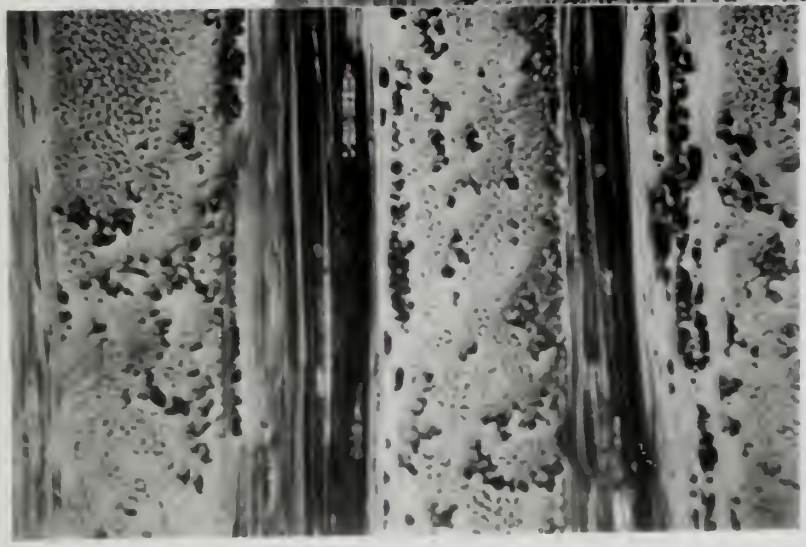

Figure 7

#11W

68,000 psi

12[illegible] Cycles

No Failure

120X

Parallel Face

Load Direction

is Vertical

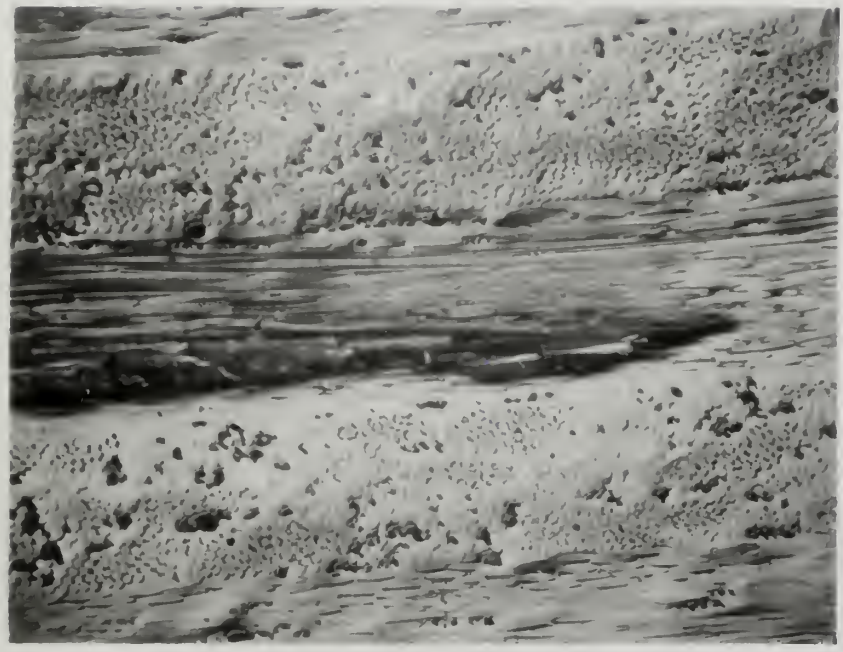

Figure [illegible]
#11W
[illegible],000 psi
120 Cycles
No Failure
120X
Perpendicular Face
Load Direction is
Out of the Page

Figure 9
#11BD
61,000 psi
$\frac{1}{2}$ Cycle
Failure
120X
Perpendicular Face
Load Direction is
Out of the Page

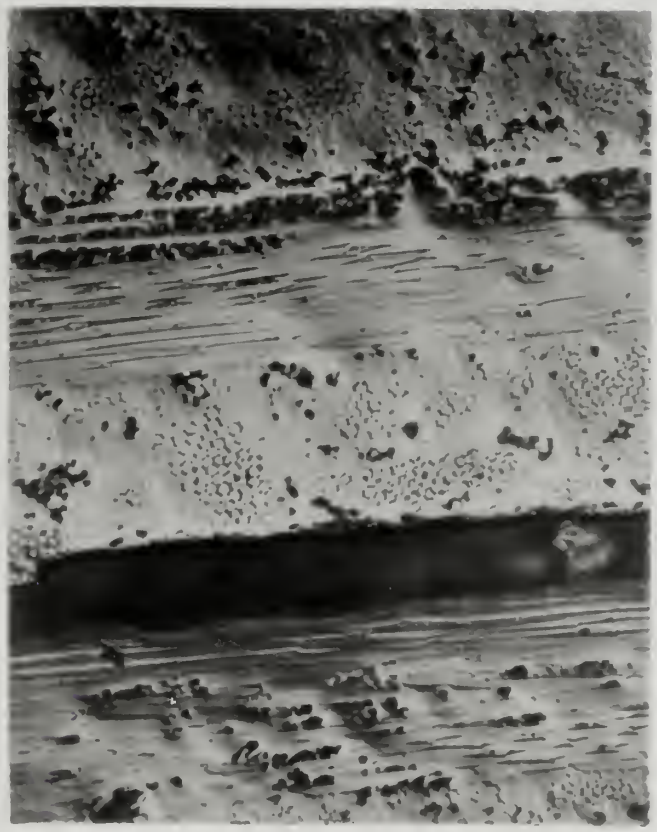

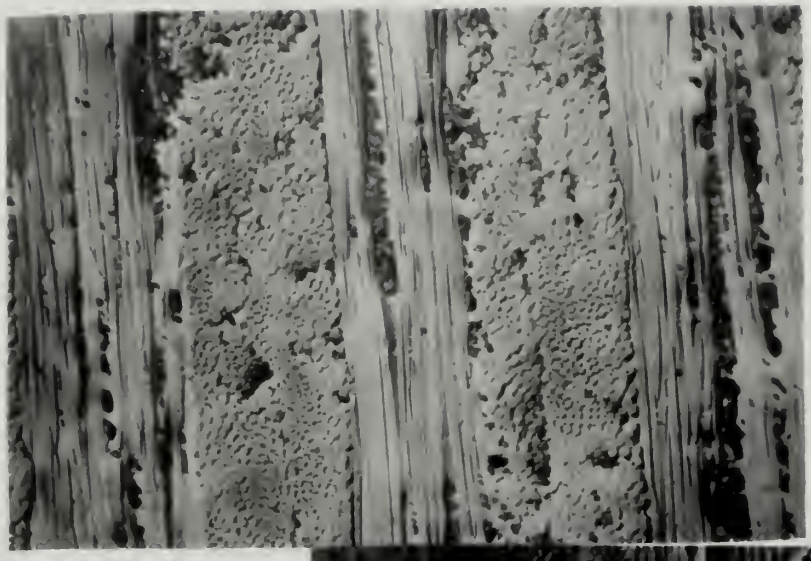

Figure 10
Laminate #10
Reference
120X
Parallel Face

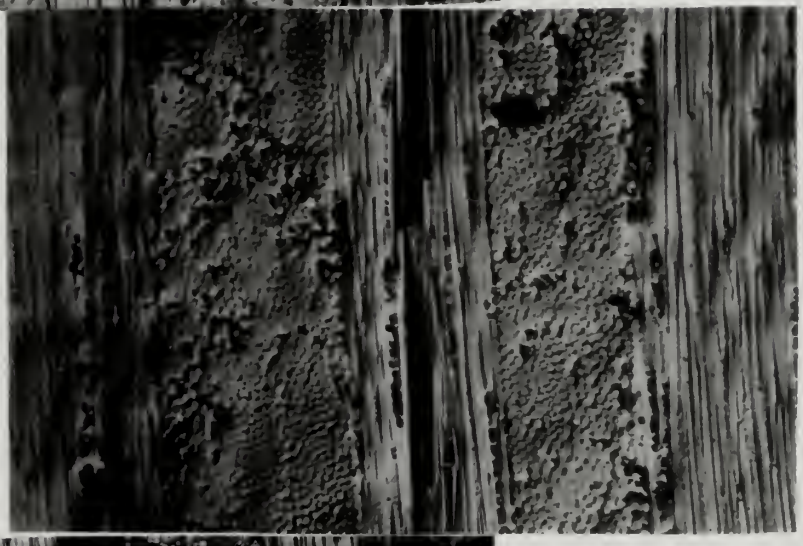

Figure 11
#10U
69,400 psi
30 Cycles
No Failure
120X
Parallel Face
Load Direction
is Vertical

Figure 12
#10N
91,000 psi
13 Cycles
Failure
120X
Perpendicular Face
Load Direction is
Out of the Page

Figure 13
Laminate #6
Reference
120X
Parallel Face

Figure 14
#11BK
70,000 psi
11 Cycles
No Failure
120X
Parallel Face
Load Direction
is Vertical

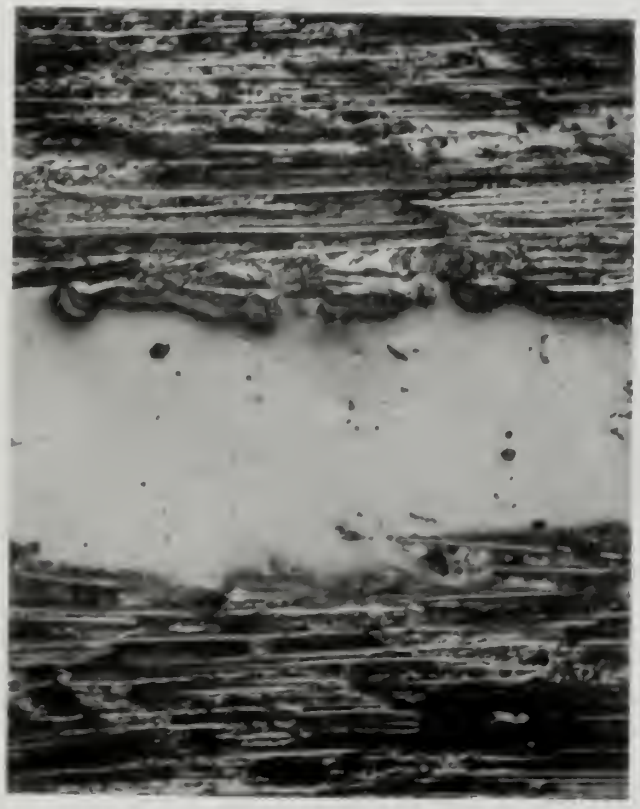

Figure 15
#11AC
67,500 psi
½ Cycle
Surface Crack
In Line Face
120X
Load Direction is
Vertical

Figure 16
#11BD
61,000 psi
½ Cycle
Failure
120X
Surface Crack
Parallel Face
Load Direction
is Vertical

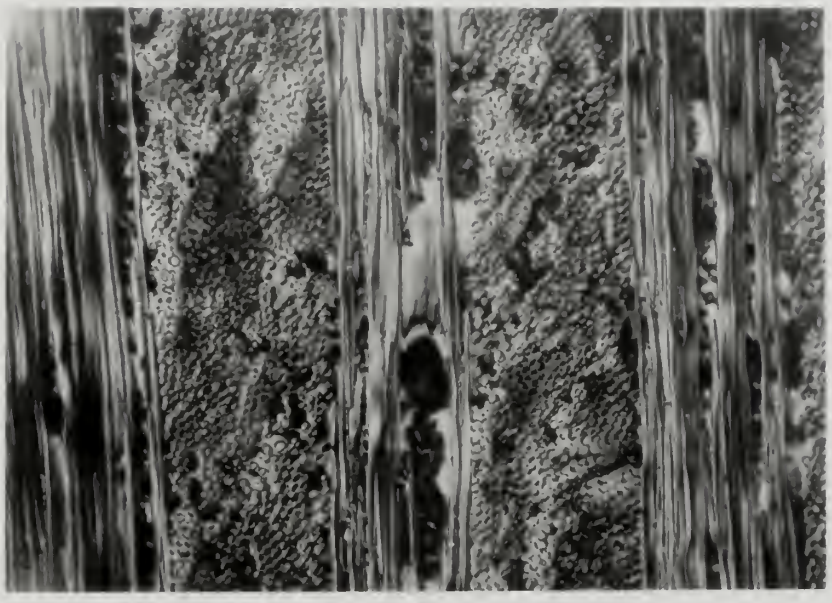

(a)

(b)

Figure 17. Specimen Number 11V (SW), Parallel Face, 120X. Reference Specimen, No Load Applied. Shown After Sea Water Immersion.

(a) Perpendicular face, showing damage in layer with fibers perpendicular to axis of load. Load applied perpendicular to plane of paper.

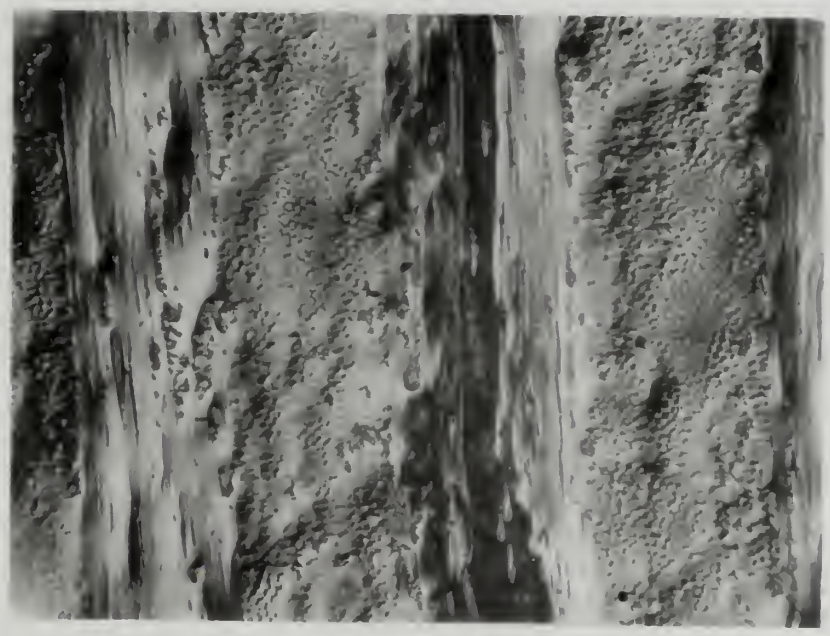

(b) Parallel face, showing damage in layer with fibers parallel to axis of load. Load applied in vertical direction.

Figure 18. Specimen 11H (SW), 120X, Fatigue Tested for 8 Cycles at 7[illegible] psi after Sea Water Immersion. Cycling Stopped Before Failure.

(a) Perpendicular face, showing interlaminar separation. Load applied perpendicular to plane of paper.

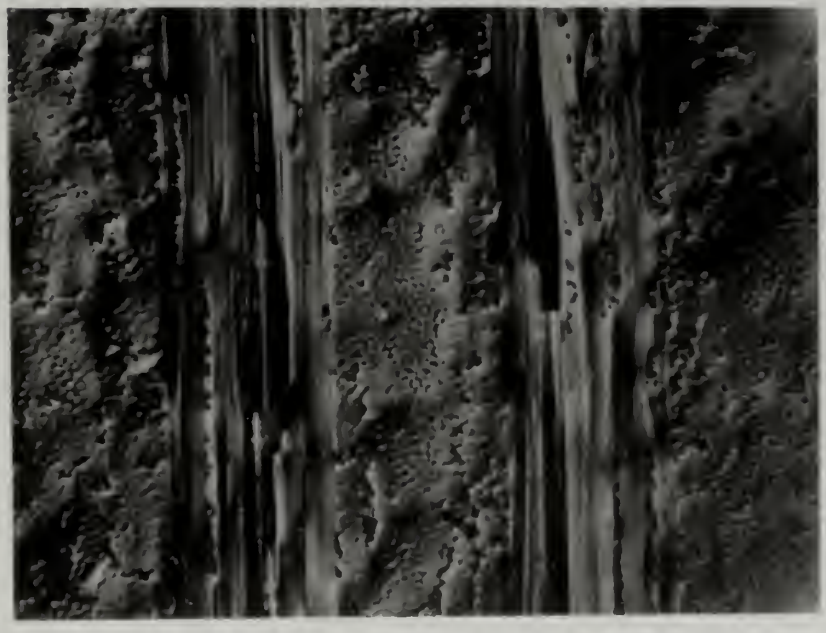

(b) Parallel face, showing damage in layer with fibers perpendicular to axis of load. Load applied in vertical direction.

Figure 19. Specimen 11P (SW), 120X, Fatigue Tested to Failure after Sea Water Immersion. Failure After 10 Cycles at 66,500 psi.

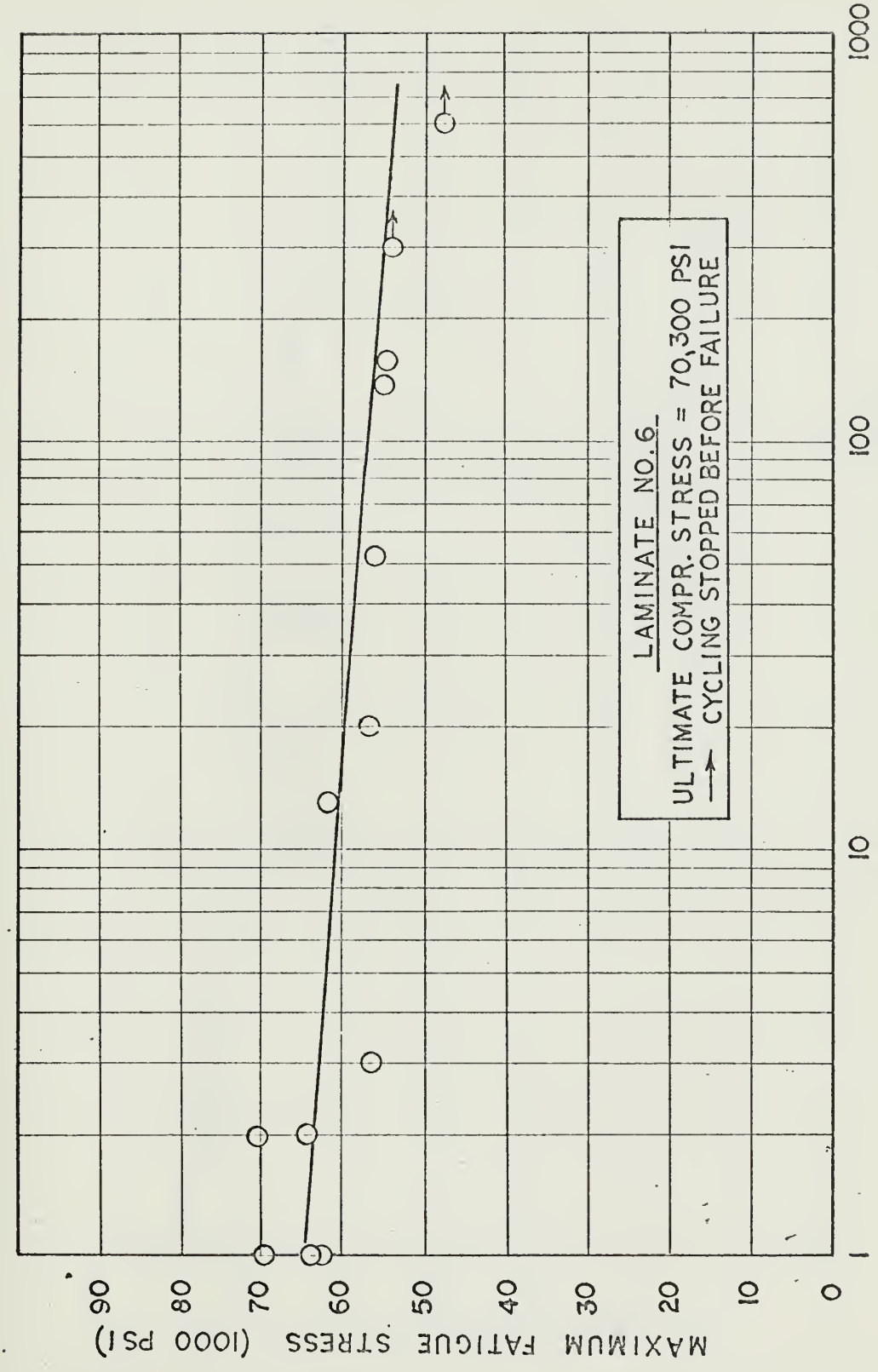

Figure 20. S-N Curve for Compressive Fatigue Test of Laminate 6, tested at 6 cycles per minute.

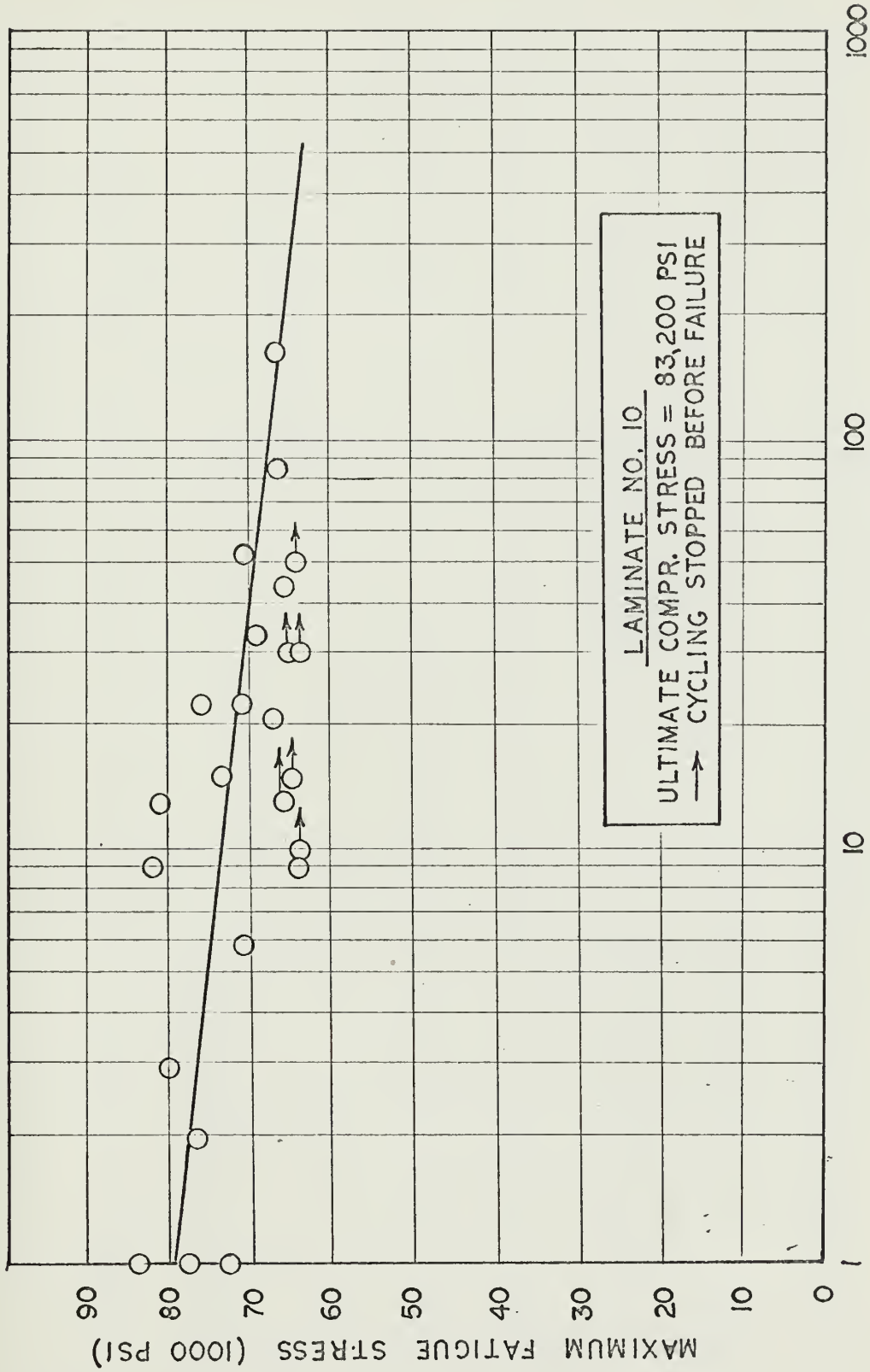

Figure 21. S-N Curve for Compressive Fatigue Test of Laminate 10, tested at 6 cycles per minute.

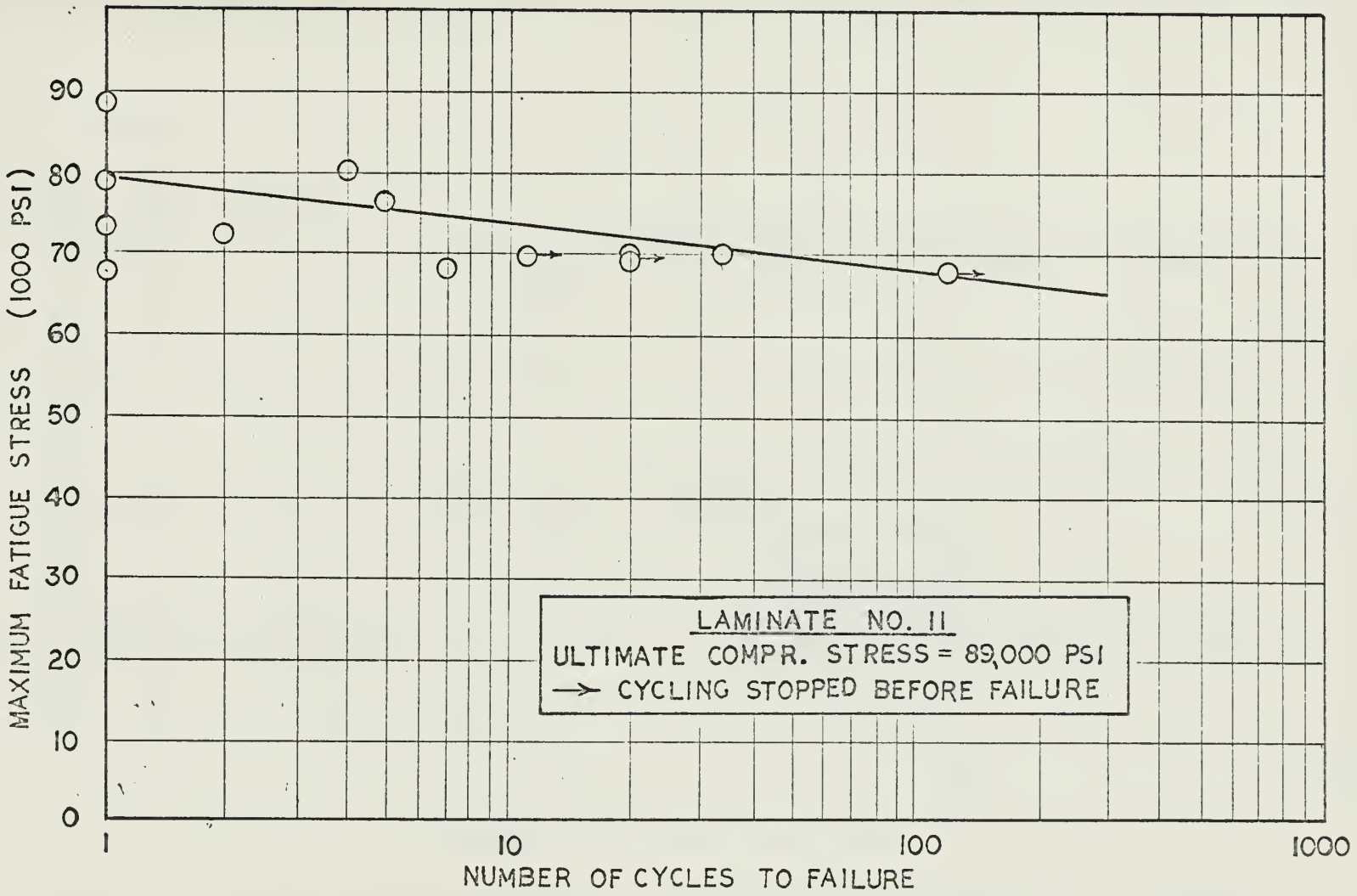

Figure 22. S-N Curve for Compressive Fatigue Test of Laminate 11, tested at 6 cycles per minute.

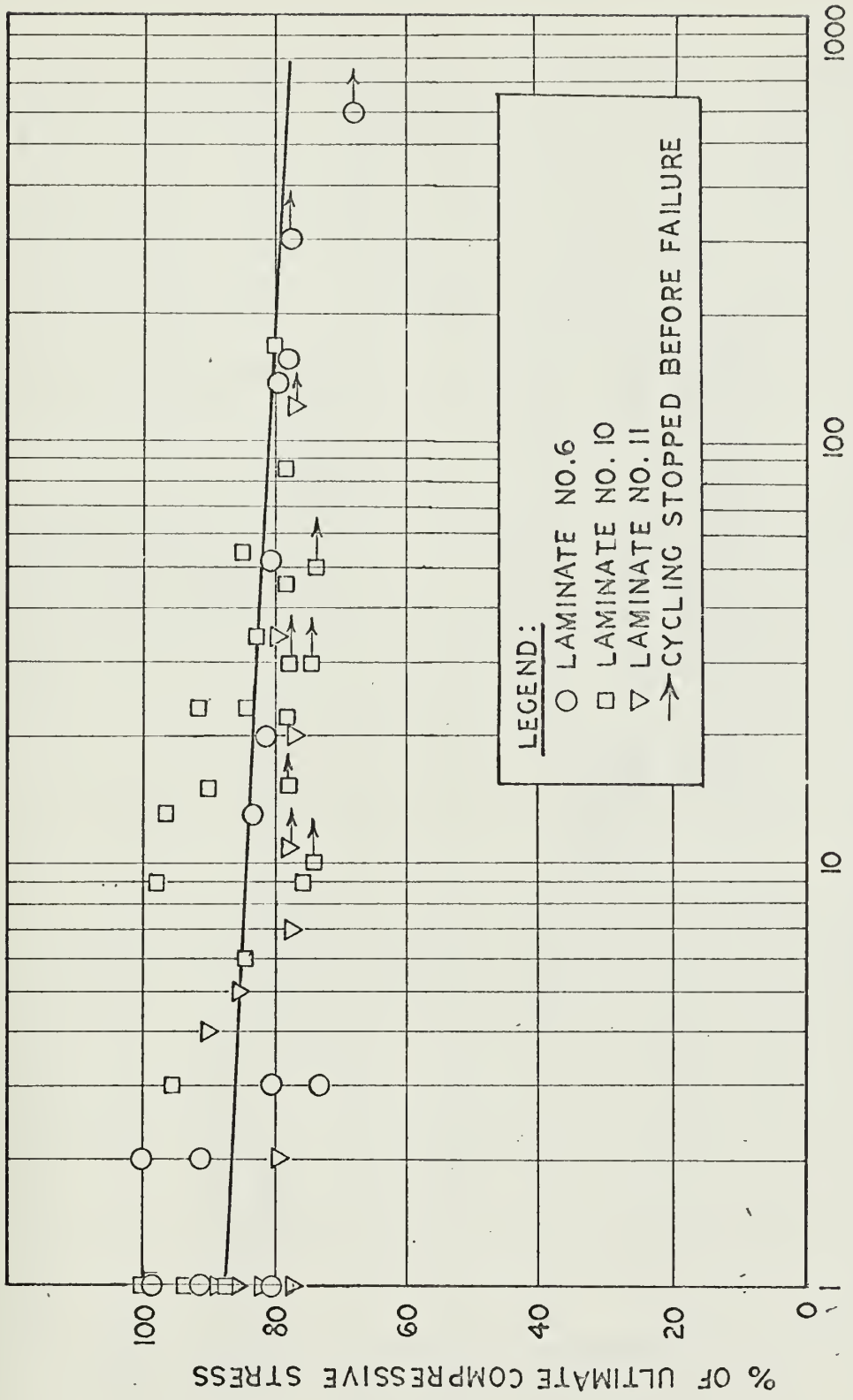

Figure 23. Combined S-N Curve for Compressive Fatigue Tests of Laminates 6 , 10, and 11, tested at 6 cycles per minute. Fatigue stress normalized to Percent of Ultimate.

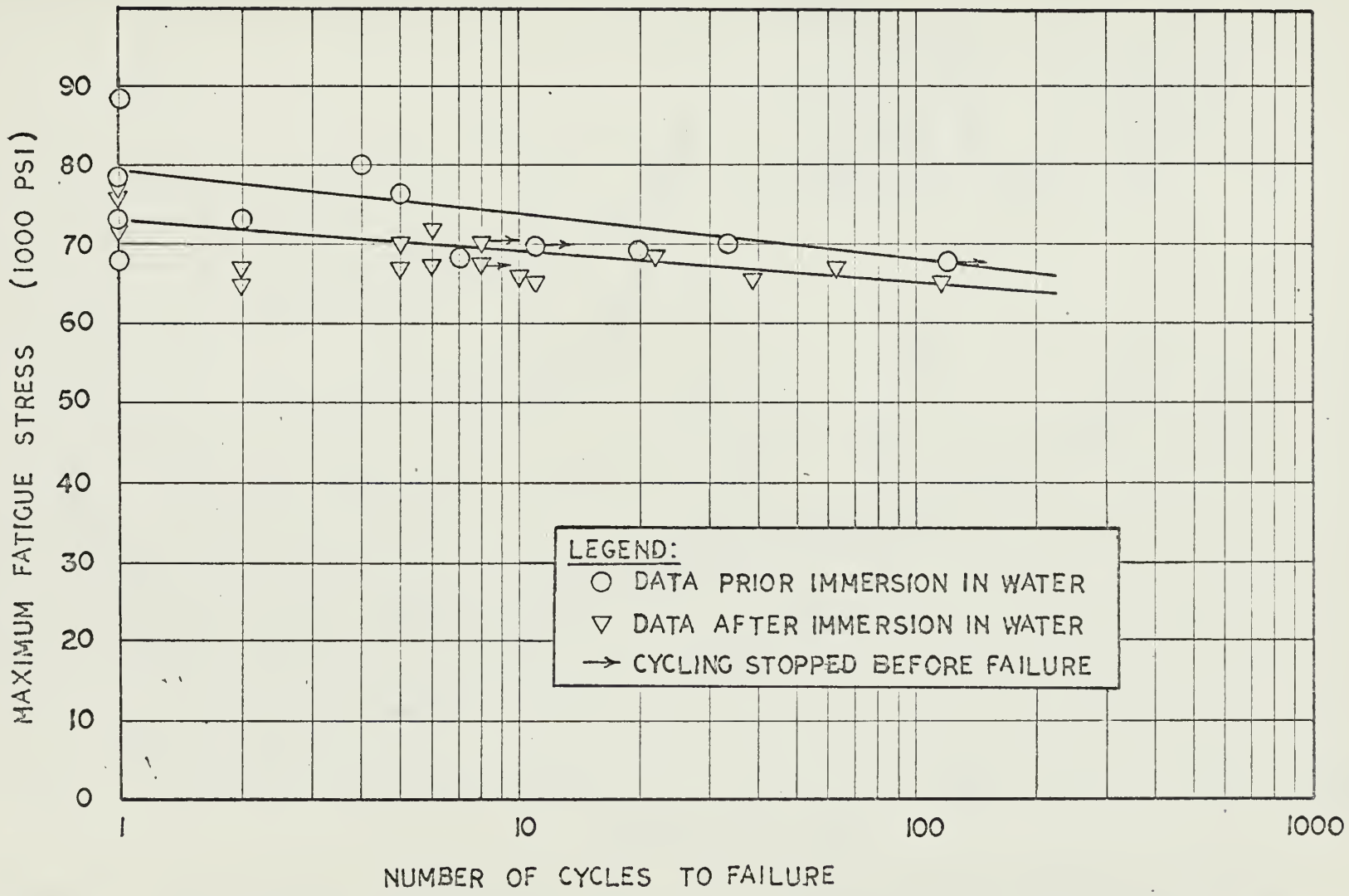

Figure 24. S-N Curves for Compressive Fatigue Tests of Laminate 11, showing effects of water immersion.

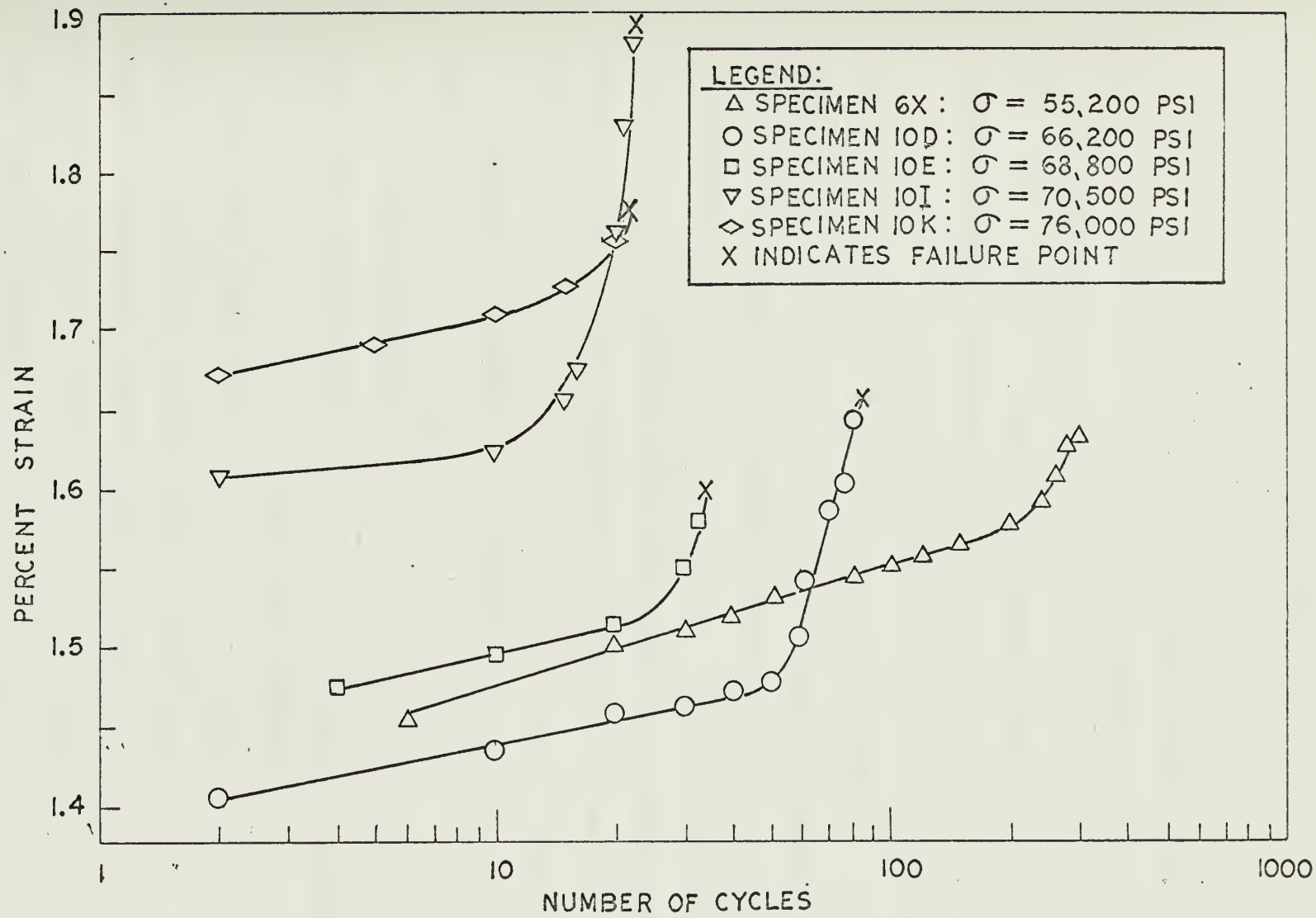

Figure 25. Strain History of Selected Specimens During Compressive Fatigue Testing at 6 cycles per Minute, Showing Sharp Increase in Strain Rate at Approximately 60% of Fatigue Life.

DISCUSSION OF RESULTS

Testing Results

In reviewing the properties of the various laminates tested, the void content, fiber volume fraction and compressive strength tend to follow Foye's hypotheses as previously expressed in Equation 6. These results are also in general agreement with Fried's inverse relationship between compressive strength and void content. (2)

The reduction in void content in Laminates 10 and 11 over that of Laminate 6 is attributed to more careful assembly techniques. The relatively high void content found in all laminates is attributed to to the use of a relatively low molding pressure (30 psi), as well as the absence of vacuum bag molding techniques. In the determination of void content, the systematic point count method, while producing significantly higher results, confirmed in a qualitative manner the results of the resin burnout method. The higher results of the point count method may be attributed to the difficulty encountered in the visual identification of voids.

The linear characteristic of the S-N curves in the low cycle range tested, and the absence of an endurance limit, are in agreement with the results of similar work found in the literature.

The average water absorption of 0.226% by weight over the 21-day immersion period is slightly higher than would be predicted using the manufacturer's data in Appendix A, and is in general agreement with the results of Fried, et. al., (1) for a high void content material under atmospheric pressure. However, Fried's findings that

"wet" and "dry" fatigue data could be clearly defined only at lower stress levels was not supported by this study. As shown in Figure 24, the reduction in fatigue strength due to water immersion is more pronounced at the higher stress levels.

The strain history data, plotted for selected specimens in Figure 25, proved to be of value as a rough indicator of proximity to fatigue failure. The characteristic "knee" in the curves at approximately 60% of fatigue life appears to be fairly consistent in all specimens tested. It is interesting to note that for Specimen 6X, for which the cycling was stopped prior to failure, the calculated fatigue life based on the "knee" occurring at the 60% point, is in excellent agreement with the S-N curve for this laminate. Similar results, though not plotted, were found for Specimen 6V.

Microscopy Results

The predominant effect observed in the microscopic examination of fatigue damage was the damage within the plies oriented parallel to the load axis (axial plies). This damage is characterized by axial separation of fibers, fracture of groups of adjacent fibers, and complete absence of fiber and matrix in elongated areas several hundred fiber diameters in length. Although many specimens exhibited an interlaminar separation damage as well, damage within the axial plies was the most frequently observed type of damage. Figures 6, 7, 11, 18(b) and 19(b) show typical examples of this type of axial damage, while interlaminar separation is observed in Figures 9, 12 and 19(a).

Before proceeding to the development of a failure mechanism, a few general observations should be made with respect to the photomicrographs. First, it should be recognized that the use of the Nomarski interferometer, while providing increased contrast and detail, emphasizes the minute variations in the level of the polished surfaces. The existence of specimen damage is indicated by the non-uniform, elongated dark areas in the photomicrographs. It is considered that the damaged fibers and matrix in these areas were removed during the polishing process, leaving a void-like space. Actual voids, resulting from the fabrication process, while varying considerably in size from one laminate to another, are generally characterized by somewhat irregular but rounded boundaries. This can be observed in the relatively small interstitial and matrix voids appearing in Laminate 11 (Figure 5) and the large general voids of Laminate 6 (Figure 13).

Another feature appearing in the photomicrographs which requires comment is the appearance of a granular substance which is readily differentiated from fibers, matrix and voids. It appears within plies oriented in both directions, but can be seen most clearly between fibers shown in their longitudinal position. It is proposed that this granular substance is the residue from preliminary polishing of sections in which various grades of polishing paper were used. It may consist of ground matrix particles, or particles of abrasive from the polishing paper, either or both of which were forced into the specimen surface by the application of excessive polishing pressure.

Development of Failure Mechanism

In developing a probable failure mechanism, one must first consider the observed tendency of fatigue damage to occur most frequently within the axial plies. It is considered that a simplified column analogy can be applied to the entire axial ply located between two transverse plies, as well as to the individual axial fibers within the axial ply. Progressive failure of individual axial fibers by local buckling, most likely in the shear or "in phase" mode, is proposed as leading to a shear type failure of the axial ply which results in transmission of cracks through the adjacent transverse plies until fracture occurs.

The individual axial "fiber column" can be considered to be supported along its length and restrained from buckling through its bonding to adjacent matrix. In an analogous manner, the axial "ply column" can be considered to be supported by and restrained from buckling through its bonding to adjacent transverse plies. Hence, a debonding mechanism must be proposed for the initial stages of fatigue damage.

The most likely debonding is that between individual axial fibers and the adjacent matrix. The compressive axial load on a specimen causes a transverse expansion due to the Poisson effect. Since the Poisson's ratio of the epoxy matrix is greater than that of the glass fibers, the matrix expands transversely more than the glass, tending to create an interfacial tensile debonding stress. The theoretical debonding stress was previously expressed in Equation 7.

In the specimens tested, the transverse expansion was most apparent near the center section. For those specimens cycled to failure, the area immediately adjacent to the failure appeared to experience the greatest expansion. The amount of expansion could be qualitatively estimated from the impressions imparted to the specimens by the contact surfaces of the support jig.

The existence of circumferential interface separation or debonding was demonstrated by Broutman through use of the electron microscope. He further pointed out that for densely packed fibers the triangular shaped matrix section between fibers becomes a highly stressed area and is subject to failure by crack propogation. (8)

The debonding between adjacent plies, more properly termed delamination, was observed to be the failure mechanism whenever the support jig was not used. The use of the support jig restricts the lateral expansion and delamination tendency. The adjacent transverse plies, then, act to support the axial "ply column" and prevent buckling of the axial ply.

The observed cases of delamination, similar to that shown in Figures 9 and 12, could be explained by the tendency of elongated voids to appear in this interlaminar area. This hypothesis is supported by the findings of Fried (2), who concluded that such voids decrease the total bonded area and may act as loci for initiating the debonding, hence they constitute the primary factor in determining compressive strength.

Fried's conclusion that the primary failure mechanism of an orthogonal material under compression is that of interlaminar

debonding is not supported by the findings of this investigation in the case of compressive fatigue. While such debonding was found to occur, the most significant damage caused by the fatigue loading was found to exist within the axial plies. In either case, the extent and distribution of voids will affect the bonding strength between fiber and matrix, as well as between adjacent plies. The results of void content calculations and ultimate compressive strength determination are in agreement with this consideration.

The strain measurements taken during the fatigue tests add additional insight into the failure process. As indicated in Figure 25, the strain rate appears to be constant with increasing cycles up to approximately 60% of fatigue life. A significant increase in strain rate is found beyond this point. It is proposed that during this first 60% of fatigue life the only significant damage occurring is that of circumferential debonding between individual fibers and matrix within axially aligned plies. This is borne out to some extent by Figure 14, in which Specimen 11BK is shown after cycling to somewhat less than 50% of expected fatigue life. No damage is apparent within the plies or at the interlaminar surface.

When the cyclic loading has progressed to the 60% point, it is proposed that the axial fiber debonding has progressed to such an extent that the "column" support offered by the matrix has degraded to the point where local fiber buckling damage starts to become significant. Such damage probably initiates within the axial plies at regions of higher void concentrations. This local fiber buckling, with its resultant higher strain rate, continues until the damage

within the axial plies results in cracks which are eventually transmitted through the transverse plies at fracture.

It is further proposed that the failure mechanism described is identical in the specimens subject to sea water immersion. The finding that immersion reduced fatigue strength could be attributed to the effect of adsorbed moisture on the E-glass fibers. Broutman and Krock (3) state that although the precise effect is still not known after years of experimentation, general agreement exists that moisture will decrease the strength of glass fibers. The high adsorption tendency of glass for water most likely results in a corrosive action which reduces the glass strength. The amount of water absorbed by the composite was shown by Fried, et. al., (1) to vary with void content.

The void content of Laminate 11 was seen to have increased somewhat by the water immersion. It is proposed that the absorbed water is concentrated within existing voids, and tends to degrade these voids by its corrosive effect. Hence, the effect of existing voids on the compressive strength of the laminate is further emphasized by the absorption of water into these voids.

CONCLUSIONS

On the basis of this investigation, the following conclusions appear to be valid for a glass fiber - epoxy matrix composite material with alternate plies assembled in an orthogonal manner:

(1) Optical microscope investigation of specimen cross-sections is a valuable technique for studying the progressive damage resulting from compressive fatigue loading.

(2) The S-N Curves for low cycle compressive fatigue show a linear decrease in fatigue strength with an increase in fatigue cycles. No endurance limit is apparent within the low cycle range tested.

(3) The compressive strength and compressive fatigue strength vary directly with fiber volume fraction and inversely with void content.

(4) A significant increase in strain rate occurs during fatigue testing at approximately 60% of fatigue life, probably associated with a significant increase in local buckling of individual fibers in plies with fibers oriented parallel to the load axis.

(5) Sea water immersion reduces the ultimate compressive strength and compressive fatigue strength of the composite, probably by absorption into and degradation of existing voids.

(6) The failure mechanism of the material when subject to compressive fatigue is probably the result of a debonding between individual fibers and matrix within the plies whose fibers are parallel to the load axis. Progressive debonding is probably

the only significant damage sustained during the initial constant strain rate period up to approximately 60% of fatigue life. Beyond this point local buckling of individual axial fibers probably causes the rapid increase in strain rate and damage within the axial plies. When cracks in the damaged axial plies are finally transmitted through the transverse plies, a slant type of shear fracture occurs. Final fracture is usually catastrophic, and is characterized by a rapid decrease in indicated load with a simultaneous loud cracking noise.

(7) Fatigue characteristics are probably a controlling factor in the application of composite materials to deep submersible structural applications.

REFERENCES

1. N. Fried, J. Kaminetsky and M. Silvergleit, "Development of Filament Wound Plastics With Enhanced Compressive Properties Through Use of Improved Resin Systems," Proceedings of 22nd Annual Conference, SPI, Reinforced Plastics Division, 1967, Section 20-B.

2. N. Fried, "The Response of Orthogonal Filament Wound Materials to Compressive Stress," Proceedings of 20th Annual Conference, SPI, 1965, Section 1-C.

3. L.J. Broutman and R.H. Krock, Modern Composite Materials, Addison-Wesley Publishing Company, Reading, Massachusetts (1967).

4. S.P. Timoshenko and J.M. Gere, Theory of Elastic Stability, McGraw-Hill, New York, 1961, p. 94.

5. B.W. Rosen, "Mechanics of Composite Strengthening," Fiber Composite Materials, American Society for Metals, 1964.

6. J.R. Lager and R. June, "Compressive Strength of Boron-Epoxy Composites," Journal of Composite Materials, Volume 3, Jan. 1969, pp. 48-56.

7. R.L. Foye, "Compression Strength of Unidirectional Composites," Paper presented at AIAA, January 1966.

8. L.J. Broutman, "Failure Mechanisms for Filament Reinforced Plastics," Modern Plastics, April 1965.

9. C.K. Cole, R.H. Cornish and J.P. Elliott, "Effect of Voids and Structural Defects on the Compressive Fatigue of Glass Reinforced Plastics," Proceedings of 21st Annual Conference, SPI, Reinforced Plastics Division, 1966, Section 17-C.

10. 3M Company Technical Data, Type 1002 Scotchply Reinforced Plastic, January 1963, St. Paul, Minnesota.

11. K.H. Boller, "Effect of Pre-Cyclic Stresses on Fatigue Life of Plastic Laminates Reinforced With Unwoven Fibers," Technical Documentary Report No. ML-TDR-64-168, Air Force Materials Laboratory, Research and Technology Division, Air Force Systems Command, Wright-Patterson Air Force Base, Ohio, Sept. 1964.

12. K. H. Boller, Fatigue Strength of Plastic Laminates Reinforced With "S" Glass Fibers," Technical Documentary Report No. AFML-TR-64-403, Air Force Materials Laboratory, Research and Technology Division, Air Force Systems Command, Wright-Patterson Air Force Base, Ohio, May 1965.

13. ASTM Test Methods, "Tenative Method of Test for Compressive Properties of Rigid Plastics," ASTM Designation D695-68T, ASTM, Philadelphia, Pa.

14. L.J. Broutman and S. Sahu, "Progressive Damage of a Glass Reinforced Plastic During Fatigue," Proceedings of 24th Annual Conference, SPI, Reinforced Plastics Division, 1969, Section 11-D.

15. W.H. Otto, "Compaction Effects in Glass Fibers," American Ceramic Society Journal, Vol 44-2, February 1961, pp.68-72.

16. 3M Company Memorandum, "Scotchply Type 1002 Resin Casting Tested per ASTM Procedures at 73°F.," 3M Company, St. Paul, Minnesota.

17. R.T. DeHoff and F.N. Rhines, Quantitative Microscopy, McGraw-Hill, New York, 1968.

18. J.E. Hilliard and J.W. Cahn, "An Evaluation of Procedures in Quantitative Metallography for Volume-Fraction Analysis," Trans. of Metallurgical Society of AIME, 221, pp.344-352, 1961.

APPENDIX A

Manufacturer's Technical Data

General Description

Material Designation	Type 1002 Scotchply
Temperature Range in Service	-60°F to 250°F
Average Uncured Thickness (in.)	0.011
Resin Content, Uncured (%)	36 % by weight
Type of Matrix	Epoxy

Physical Properties, Cured Laminate

Flammability (in/min)	0.10
Barcol Hardness	70
Rockwell Hardness (M Scale)	100 - 108
Specific Gravity	1.84
Molded thickness, one ply (in)	0.010
Wet Strength Retention (%, 2 hr. boil)	86

Mechanical Properties (Stress Angle 0°, Temperature 70°F)

	Unidirectional Laminate	Crossplied Laminate
Flexure Strength (psi x 10^3)	165	120
Modulus in Flexure (psi x 10^6)	5.3	3.5
Tensile Strength (psi x 10^3)	160	75
Modulus in Tensile (psi x 10^6)	5.7	3.7
Compressive Strength, Edge (psi x 10^3)	90	75
Izod Impact, Edge (ft.lb./in.notch)	60.8	35.2
Interlaminar Shear Strength (psi x 10^3)	4.3	4.1

Chemical Properties

Water Absorption, 24 hour immersion (%)	0.05
Water Absorption, 7 day immersion at 70°F :	
Change in Weight (%)	+ 0.17
Change in Thickness (%)	+ 0.09
Flexural Strength (psi x 10^3)	109
Specific Heat (cal/gm-°C)	0.21

APPENDIX B

TABLE 1. LAMINATE 6 FATIGUE DATA

Ultimate Compressive Stress = 70,300 psi

SPECIMEN	MINIMUM AREA (IN^2)	FATIGUE LOAD (LB) MAX	MIN	FATIGUE STRESS (PSI) MAX	MIN	CYCLES TO FAIL
6G	.0701	3980	---	56,800	---	1/2
6H	.0719	4980	---	69,500	---	1/2
6J	.0709	4980	800	70,300	11,300	2
6K	.0774	5000	400	64,600	5,180	2
6L	.0746	4100	100	55,000	1,340	154
6M	.0758	4850	---	64,000	---	1/2
6N	.0775	4800	30	62,000	390	13
6O	.0731	4600	---	62,900	---	1/2
6Q	.0715	4050	200	56,700	2,790	3
6S	.0736	4100	150	55,600	2,040	136
6T	.0731	3720	150	50,800	2,050	3
6V	.0721	3460	140	47,900	1,940	600*
6W	.0730	4100	120	56,900	1,670	20
6X	.0743	4100	140	55,200	1,880	300*
6Y	.0695	3920	100	56,400	1,440	1/2

* Indicates cycling stopped before failure

TABLE 2. LAMINATE 10 FATIGUE DATA

Ultimate Compressive Stress = 83,200 psi

SPECIMEN	MINIMUM AREA (IN^2)	FATIGUE LOAD (LB) MAX	FATIGUE LOAD (LB) MIN	FATIGUE STRESS (PSI) MAX	FATIGUE STRESS (PSI) MIN	CYCLES TO FAIL
10A	.0617	5140	--	83,200	--	1/2
10B	.0643	4200	140	65,300	2180	45
10C	.0667	4220	80	63,200	1200	9
10D	.0653	4320	100	66,200	1530	84
10E	.0652	4480	100	68,800	1530	34
10F	.0635	4500	100	70,700	1570	54
10G	.0637	4220	60	66,200	940	22
10H	.0615	4320	140	70,500	2280	6
10I	.0641	4520	100	70,500	1560	23
10J	.0568	4190	60	73,800	1050	15
10K	.0607	4620	60	76,000	990	23
10L	.0550	4010	--	72,400	--	1/2
10M	.0608	4850	60	79,700	990	3
10N	.0609	4920	60	81,000	990	13
10O	.0575	4380	--	76,300	--	2
10P	.0640	4250	80	66,500	1250	167
10Q	.0601	4650	--	77,500	--	1/2
10S	.0605	4950	60	81,800	990	9
10U	.0553	3600	100	65,200	1815	30 *
10Z	.0548	3400	80	62,000	1460	30 *
10AA	.0489	3180	60	65,000	1225	15 *
10AB	.0534	3490	80	65,400	1500	13 *
10AF	.0567	3500	80	61,900	1410	10 *
10AG	.0525	3280	80	62,600	1520	50 *

* Indicates cycling stopped before failure

TABLE 3. LAMINATE 11 FATIGUE DATA

SPECIMEN	MINIMUM AREA (IN^2)	FATIGUE LOAD (LB) MAX	FATIGUE LOAD (LB) MIN	FATIGUE STRESS (PSI) MAX	FATIGUE STRESS (PSI) MIN	CYCLES TO FAIL
A. SPECIMENS TESTED WITHOUT SEA WATER IMMERSION						
Ultimate Compressive Stress = 89,000 psi						
11A	.0597	5300	--	89,000	--	1/2
11W	.0604	4100	80	68,000	1320	120 *
11X	.0691	4200	80	71,000	1350	2
11Y	.0602	4220	60	70,000	1000	34
11Z	.0605	4160	80	68,900	1320	7
11AA	.0587	4700	200	80,200	3410	4
11AB	.0626	4760	40	76,100	640	5
11AC	.0604	4060	--	67,500	--	1/2
11AD	.0619	4260	100	69,000	1620	20
11BA	.0605	4760	--	79,000	--	1/2
11BC	.0592	4320	--	73,000	--	1/2
11BD	.0610	3720	--	61,000	--	1/2
11BE	.0604	4200	100	69,400	1650	20 *
11BI	.0602	4580	--	76,100	--	1/2
11BK	.0586	4100	70	70,000	1195	11 *
B. SPECIMENS TESTED AFTER SEA WATER IMMERSION						
Ultimate Compressive Stress = 77,800 psi						
11C(SW)	.0625	4520	--	72,300	--	1/2
11D(SW)	.0598	4040	100	67,600	1670	62
11E(SW)	.0609	4200	120	69,000	1970	22
11F(SW)	.0598	4260	80	71,200	1340	6
11G(SW)	.0600	4040	100	67,400	1670	2
11H(SW)	.0597	4200	100	70,300	1670	8 *
11J(SW)	.0592	4160	200	70,200	3380	5
11L(SW)	.0600	4080	80	68,000	1330	6
11M(SW)	.0600	3890	100	64,900	1670	2
11N(SW)	.0597	4070	100	68,200	1675	8 *
11O(SW)	.0600	4030	100	67,200	1670	5
11P(SW)	.0602	4000	140	66,500	2320	10
11Q(SW)	.0598	3920	80	65,500	1340	11
11R(SW)	.0602	3960	100	65,800	1660	39
11S(SW)	.0592	3850	200	65,000	3380	114
11T(SW)	.0600	4600	--	76,600	--	1/2
11U(SW)	.0623	4850	--	77,800	--	1/2

* Indicates cycling stopped before failure

TABLE 4. STRAIN DATA FOR SELECTED SPECIMENS

SPECIMEN 10D: L = 2.493 in (Failure: 84 cycles @ 66,200 psi)

N	ΔL (in.)	ΔL/L x 100%
2	.0350	1.405
10	.0358	1.435
20	.0364	1.460
30	.0365	1.463
40	.0367	1.472
50	.0369	1.480
58	.0376	1.508
60	.0385	1.543
70	.0396	1.588
75	.0400	1.605
80	.0410	1.643
84	.0412	1.654

SPECIMEN 10E: L = 2.495 in. (Failure: 34 cycles @ 68,800 psi)

N	ΔL (in.)	ΔL/L x 100%
4	.0368	1.475
10	.0373	1.495
20	.0378	1.515
30	.0387	1.550
32	.0394	1.579
34	.0398	1.595

SPECIMEN 10I: L = 2.494 in. (Failure: 23 cycles @ 70,500 psi)

N	ΔL (in.)	ΔL/L x 100%
1	.0392	1.572
2	.0404	1.610
10	.0405	1.624
15	.0412	1.653
16	.0418	1.675
20	.0440	1.764
21	.0457	1.830
22	.0469	1.880
23	.0473	1.897

SPECIMEN 10K: L = 2.496 in. (Failure: 23 cycles @ 76,000 psi)

N	ΔL (in.)	ΔL/L x 100%
2	.0417	1.672
5	.0422	1.690
10	.0426	1.710
15	.0431	1.728
20	.0438	1.756
22	.0443	1.778

SPECIMEN 6X: L = 2.542 in. (No Failure, stopped at 300 cycles)

N	ΔL (in.)	ΔL/L x 100%
6	.0370	1.455
20	.0382	1.502
30	.0384	1.510
40	.0387	1.520
50	.0390	1.533
60	.0391	1.537
80	.0393	1.544
100	.0395	1.552
120	.0396	1.557
150	.0399	1.568
160	.0401	1.575
200	.0402	1.580
240	.0405	1.591
260	.0409	1.609
280	.0414	1.628
300	.0415	1.631

TABLE 5. WEIGHT DATA FOR SEA WATER IMMERSION TEST

SPECIMEN	WEIGHT BEFORE IMMERSION (mg)	WEIGHT AFTER IMMERSION (mg)	WEIGHT GAIN mg	WEIGHT GAIN %
11C (SW)	7753	7764	11	.142
11D (SW)	7448	7467	19	.255
11E (SW)	7478	7503	25	.334
11F (SW)	7449	7463	14	.188
11G (SW)	7528	7549	21	.278
11H (SW)	7466	7489	23	.307
11I (SW)	7503	7522	19	.253
11J (SW)	7467	7491	24	.321
11K (SW)	7628	7645	17	.223
11L (SW)	7493	7513	20	.267
11M (SW)	7496	7517	21	.280
11N (SW)	7518	7533	15	.199
11O (SW)	7487	7500	13	.173
11P (SW)	7473	7490	17	.227
11Q (SW)	7428	7439	11	.148
11R (SW)	7468	7485	17	.228
11S (SW)	7377	7392	15	.202
11T (SW)	7683	7693	10	.130
11U (SW)	7693	7706	13	.169
11V (SW)	7346	7362	16	.208
AVERAGE WEIGHT CHANGE			17.1 mg	.226 %

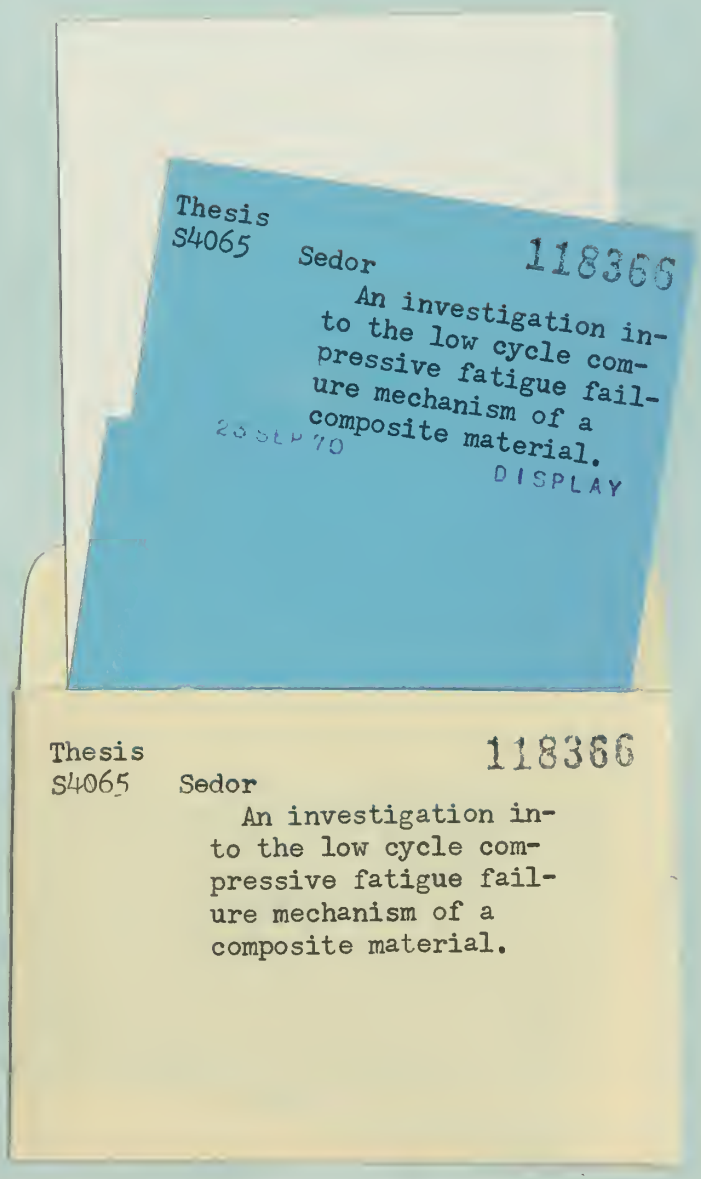

Thesis
S4065
Sedor
118366
An investigation into the low cycle compressive fatigue failure mechanism of a composite material.